

Article

Numerical Investigation of Rotating Instability Development in a Wide Tip Gap Centrifugal Compressor [†]

Xavier Flete ^{1,2,*} , Nicolas Binder ² , Yannick Bousquet ²  and Sandrine Cros ¹

¹ Liebherr-Aerospace Toulouse SAS, 408 Avenue des Etats Unis, 31016 Toulouse, France

² ISAE-SUPAERO, 10 Av. Edouard Belin, 31400 Toulouse, France; nicolas.binder@isae-supero.fr (N.B.); yannick.bousquet@isae-supero.fr (Y.B.)

* Correspondence: xavier.flete@isae-supero.fr

[†] This manuscript is an extended version of our paper published in the proceedings of the 15th European Turbomachinery Conference, Budapest, Hungary, 24–28 April 2023.

Abstract: In the current study, full-stage unsteady simulations were performed to investigate rotating instability inception mechanisms in a particularly large tip clearance centrifugal compressor with a vaneless diffuser and a volute. Four operating points along a speed line were analysed to understand the influence of the mass flow reduction on flow structures. Close to the peak efficiency, an unsteady interaction between the tip clearance vortices and splitter blades was observed. Considering other studies, the influence of the tip gap size was analysed. Then, a large-scale vortex shedding from the leading edges of the main blades was detected when the stage operated near the maximum pressure ratio. It was demonstrated that shed vortices were caused by the combination of the radial gradient of the tangential velocity under the tip vortex and the reverse backflow near the casing. Previous studies on axial compressors refer to these vortical structures as backflow vortices. These vortices cause a significant increase in the incidence angle in the tip region.

Keywords: backflow vortices; centrifugal compressor; rotating instability; tip leakage flow; wide tip clearance



Citation: Flete, X.; Binder, N.; Bousquet, Y.; Cros, S. Numerical Investigation of Rotating Instability Development in a Wide Tip Gap Centrifugal Compressor. *Int. J. Turbomach. Propuls. Power* **2023**, *8*, 25. <https://doi.org/10.3390/ijtp8030025>

Academic Editor: Antoine Dazin

Received: 8 June 2023

Revised: 20 June 2023

Accepted: 13 July 2023

Published: 1 August 2023



Copyright: © 2023 by the authors. Licensee MDPI, Basel, Switzerland. This article is an open access article distributed under the terms and conditions of the Creative Commons Attribution (CC BY-NC-ND) license (<https://creativecommons.org/licenses/by-nc-nd/4.0/>).

1. Introduction

The automotive industry is still keen on the design of centrifugal compressors with an ever-increasing operating range and compactness. However, the tip clearance size remains constant due to the technology choice, while the impeller size decreases. As a result, new automotive compressors have relatively large tip gaps compared to the blade span. But, as shown in the literature, tip leakage flows have a predominant role in the emergence of flow instabilities.

Inoue and Kuroumaru [1] demonstrated that in an axial compressor, the interaction between the tip leakage flow and the main flow leads to the formation of tip leakage vortices. As the clearance increases, a reverse flow due to the vortex grows near the casing wall. Further works of Inoue et al. [2–4] showed that when the tip gaps were large, the flow at the leading edge became unsteady and degenerated into a leading edge separation. They proposed a theory based on a tornado-like vortex extending radially inward, from the shroud to the blade's suction side, which leads to the onset of short length-scale stall cells. Other tip clearance vortices were observed by März et al. [5] in pre-stall conditions. These vortical structures, confined to the tip region of a rotor, moved from the suction side to the pressure side of the neighbouring blade. According to Mailach et al. [6] and the works cited above, these unsteady disturbances are identified as 'rotating instabilities' whereby the compressor operates in 'mild stall' conditions. In 2008, Vo et al. [7] suggested that such a tip flow could be linked to the onset of short length-scale rotating stalls. This assumption was confirmed by numerical investigations from Pullan et al. [8], which demonstrated that the short length-scale stall is caused by a separation at the leading edge due to a high

incidence causing the emergence of tornado vortices. They also described the propagation of these structures according to the mechanisms observed by März by adding the idea of a self-sustaining mechanism.

Bousquet et al. [9] observed similar vortex shedding at the leading edge of a centrifugal compressor with a vaned diffuser without a volute in near-stall conditions. The interaction between the leading edge separation and the incoming flow resulted in a Kelvin–Helmholtz instability inducing the tornado vortex shedding. However, in this configuration, the vortices' trajectory was such that no short length-scale rotating disturbances were observed. More recently, a similar Kelvin–Helmholtz mechanism was mentioned by Cao et al. [10] to explain the onset of massive vortex shedding from a tip leakage flow breakdown process close to the leading edges. This numerical and experimental investigation of a centrifugal compressor with a vaneless diffuser and a volute outlines the emergence of vortex tubes that propagate circumferentially and that strongly interact with the next blade's leading edge. The main difference between Bousquet et al.'s observations and those of Cao et al. is the direction of the vortical structures. Those mentioned by Cao are tubes oriented in the blade-to-blade direction and depend on the downstream pressure field imposed by the volute's tongue. Such phenomena are reminiscent of the residuals of the broken main tip leakage vortex described by Iwakiri et al. [11] as a result of single-impeller simulations. Like the previous authors, Tomita et al. [12] linked these tip leakage flow instabilities to the degradation of the compressor performances. However, they also demonstrated that the tip leakage vortex breakdown can stabilise the flow field and increase the operating range at a low mass flow by accelerating the incoming flow near the hub, unaffected by the vortical structures.

As an extended version of the study introduced by Flete et al. [13] at the 15th European Turbomachinery Conference, the present work complements the recent studies on flow instabilities in centrifugal compressors belonging to the turbocharger family in the following ways:

- It highlights the interaction between tip leakage vortices and splitter blades (related to a wide tip clearance), which degrades performances near the peak efficiency.
- It proposes an inception mechanism for vortex tube shedding described by Cao et al. [10] according to the investigation carried out by Chen et al. [14].

First, the studied compressor and numerical method are introduced. The next part presents a detailed analysis of the flow topology's gradual evolution caused by the mass flow reduction. Full-stage simulations are used to highlight the tip clearance vortex behaviour and the emergence of rotating instabilities in near-stall conditions. In particular, the propagation of massive vortices oriented perpendicular to the streamwise direction highly similar to those observed by Cao et al. [10] is described. Considering the velocity distribution, these vortical structures are identified as backflow vortices according to previous studies on axial machines. However, the inception mechanisms proposed by Cao et al. for centrifugal configurations and Chen et al. for axial configurations are different, and questions remain about the origin of such structures. Hence, the last part of the present study aims to clarify the development process of this vortex tube shedding.

2. Methodology

2.1. Test Case Geometry

The studied centrifugal compressor was designed by Liebherr-Aerospace Toulouse to supply air into an automotive fuel cell. Two of the most important requirements are a wide operating range and a small diameter. To meet these specifications, an impeller with splitter blades followed by a short vaneless diffuser and a volute was designed. Considering the flow field in choke conditions, the leading edges of the splitter blades are located at a relative meridional position of $M_x = 0.31$. This metric was defined based on the leading edges of the main blades ($M_x = 0$) until the trailing edges ($M_x = 1$). Numerical simulations were performed on the full-stage configuration shown in Figure 1. Table 1 describes the main compressor operating parameters. The impeller's particularity is the

wide tip clearance changing from the leading edge (6% of the blade span) to the trailing edge (18%).

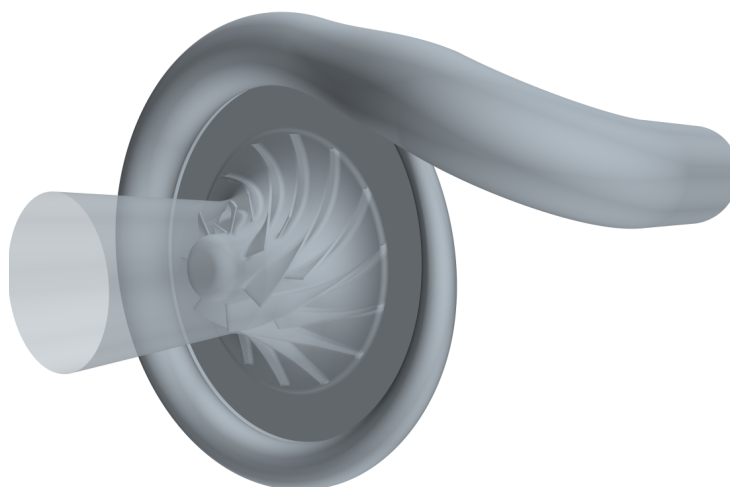


Figure 1. Computational domain.

Table 1. Main compressor features.

Parameter	Value
Blade number	7 + 7
Design rotation rate	100 krpm
Design mass flow rate	0.1 kg/s
Design pressure ratio	2
Diffuser radius ratio	1.4
Diffuser width ratio	0.07

2.2. Flow Solver

Simulations were carried out by Siemens, STAR-CCM+ using a finite volume solver, and thus, the three-dimensional unsteady compressible Reynolds-averaged Navier–Stokes equations were solved on unstructured meshes. The eddy viscosity was computed with the two-equation turbulence model $k - \omega$ SST from Menter [15]. This improved version of the original $k - \omega$ combined the good near-wall performances for boundary layers under adverse pressure gradients with the $k - \epsilon$ accuracy in free stream. A coupled flow solver was used to solve the conservation equations for mass and momentum simultaneously using a pseudo-time-marching approach. The convective and diffusive fluxes were computed with an implicit second-order upwind scheme. The time-marching was performed with an implicit second-order discretisation scheme, and governing equations were solved in the absolute reference frame to avoid artificial dissipation leading to a nonphysical rotational flow in the far field region. Each impeller revolution was described by 860 physical time steps, corresponding to 122 time steps per the main blade's passage, and 30 inner iterations were carried out at each time step.

2.3. Mesh

The full-annulus computational domain was discretised with a polyhedral unstructured mesh using near-wall prism layer meshing. The size of the first cell was set to $1.5 \mu\text{m}$, ensuring a normalised wall distance y^+ below 1.3 and mostly between 0 and 0.6. After several mesh convergence studies, the best compromise between computational time and solution accuracy was found for 48×10^6 cells in the impeller with an average of 33 cells in the tip gap's height. The vaneless diffuser and the volute were discretised into 14×10^6 cells. The information transfer between the impeller and the diffuser was handled

by a sliding-mesh interface, which was considered the most accurate method for simulating rotor-stator interactions.

2.4. Boundary Conditions

Stagnation conditions are uniformly applied to the inlet section. This method imposes the total pressure, temperature and flow direction and calculates other quantities using the isentropic relations. A study from Kulak et al. [16] demonstrated that a mass flow boundary condition tends to over-stabilise the flow and, thus, stifles initiations of instabilities. Furthermore, a uniform static pressure outlet condition prevents one from reaching a lower mass flow than the highest of the zero slope section. Hence, all the simulations in this study used a throttle law as an outlet condition.

This condition updates the outlet static pressure P_{Sout} at each time step according to the following relation:

$$P_{Sout}(t + \Delta t) = P_{S0} + \lambda \cdot \dot{m}(t)^2 \quad (1)$$

where P_{S0} is the reference static pressure, λ the throttle parameter and \dot{m} the mass flow rate through the exit section. Such a boundary condition allows regulation of the outlet pressure according to the mass flow rate and gives enough freedom to move along the flat part of the characteristic curve.

2.5. Validation

A global performance validation was conducted at Liebherr Aerospace. The stage outlet static pressure was measured downstream of the volute. Hence, the comparison between measurements and numerical data is based on a total-to-static pressure ratio normalised by the local maximum value and plotted as a function of the corrected mass flow rate. Figure 2 shows good agreement between the experiment and numerical simulations for a rotation speed set to 97% of the one investigated in the present paper. Moreover, the stability limit is reached at a similar mass flow rate. This last finding demonstrates the reliability of the numerical method used to describe the stage destabilisation mechanisms.

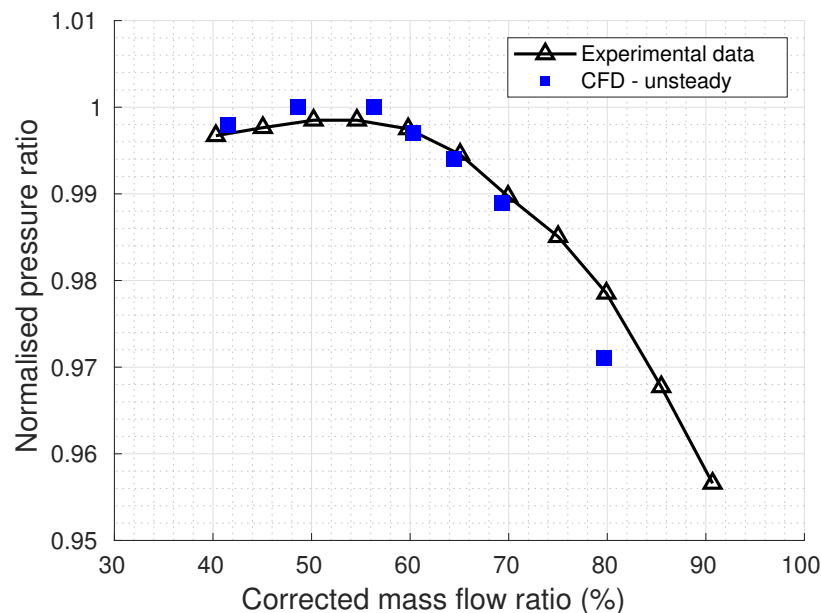


Figure 2. Comparison of experimental data and CFD results.

3. Unsteady Phenomenon near the Peak Efficiency

Four operating points (OP1, OP2, OP3 and OP4) along a speed line describe the development of instabilities in the impeller. The first operating point, OP1, illustrates the flow field in the impeller of the present compressor at design conditions. The second one, OP2, corresponds to the mass flow rate at which the tip leakage vortices hit the splitter blades' leading edges, causing unexpected unsteady behaviour near the peak efficiency. By reducing the mass flow, the compressor operates at OP3, where vortex tubes similar to those observed by Cao et al. emerge under the tip leakage vortices. Finally, the last described operation point OP4 shows the flow field topology in stall conditions. Each one is located in Figure 3, representing the stage total-to-total pressure ratio and the isentropic efficiency as a function of mass flow rate. These quantities are normalised by their respective mean values at the peak efficiency.

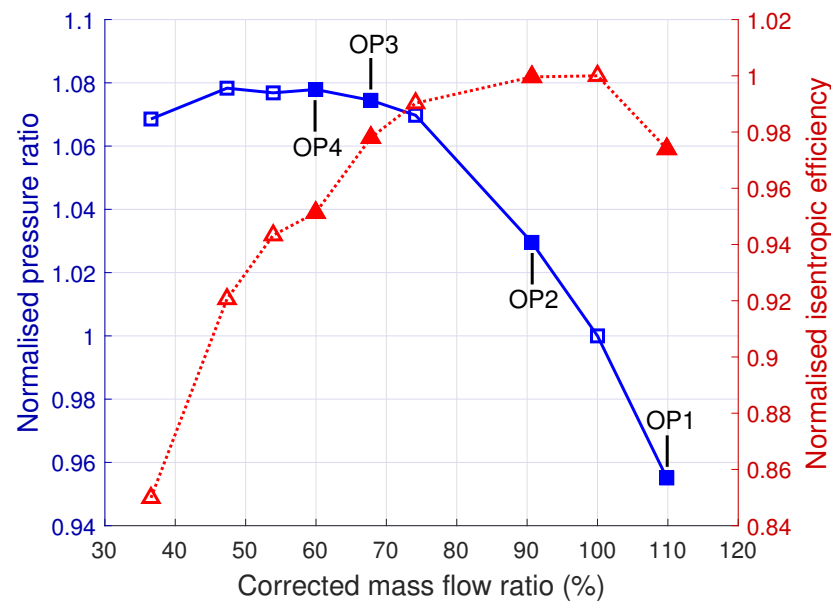


Figure 3. Studied operating points' locations on the compressor characteristic.

3.1. Flow Structures near Choke Conditions

At the highest mass flow rate OP1, the strong tip leakage flow is confined to the lower part of the half-passage near the trailing edges ($M_x > 0.65$). The recirculation from the leakage flow in the passage leads to an accumulation of low-momentum fluid near the casing wall, which, associated with the adverse pressure gradient from the vaneless diffuser, causes a near-shroud backflow in the impeller outlet tip region. However, this tip reverse flow weakens in the meridional direction before reaching the splitter blade's leading edges. Except for the trailing edge vicinity, the flow field is mostly steady. By using λ_2 criterion, it is possible to visualise the vortical structures in the impeller. λ_2 is the second eigenvalue of the sum of strain-rate tensors squared and the spin tensor squared when sorted from minimum to maximum. According to Jeong and Hussain [17], its negative values can be interpreted as vortex regions, while values equal to or greater than zero have no physical significance. Instantaneous iso-surfaces of λ_2 are shown in Figure 4. They highlight fully developed tip leakage vortices (TLV) that roll up midway between the main and the splitter blades' leading edges and extend until the downstream half-passage. In these half-passages, another tip leakage vortex emerges from the splitter blade's tip gap. At this operating point, the two wide structures are steady and do not appear to interact.

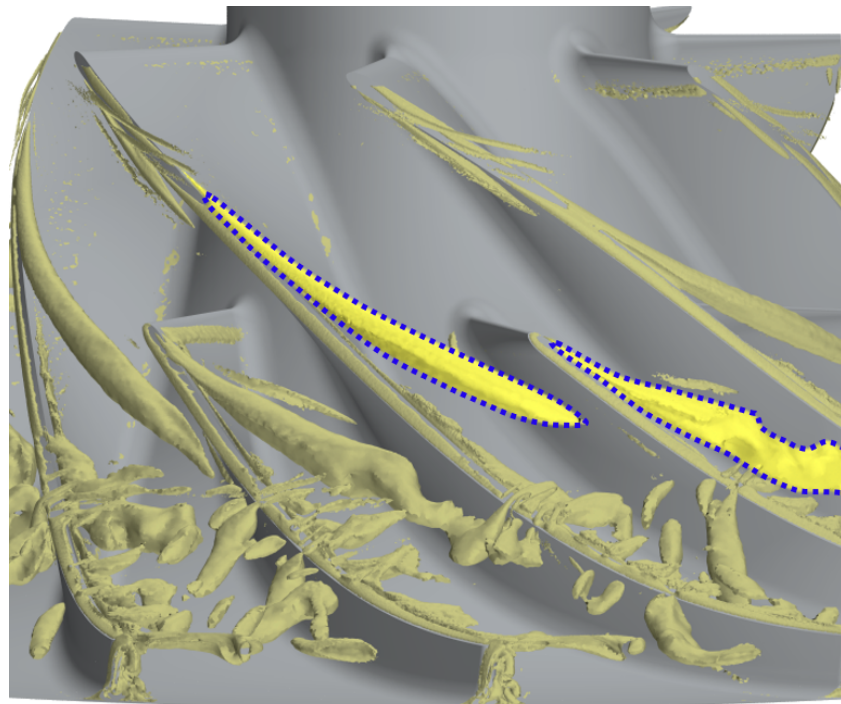


Figure 4. Iso-surfaces of λ_2 criterion at OP1.

At OP2, the strong leakage flow region overtakes the splitter blades' leading edges due to the adverse pressure gradient increase. Thus, the interface between the tip clearance and the underlying incoming flow is located diagonally between $M_x = 0.1$ and $M_x = 0.25$. Figure 5 shows that in this configuration, the initial rolling-up positions of the tip leakage vortex have migrated, and the trajectories have straightened upstream in such a way that the vortices from the main blades hit the splitter blade's leading edges, thus breaking the second TLV. Even if the upper part of the passage ($M_x < 0.3$) is mainly stationary, the interaction between the main blade TLV's tail and the splitter blade's leading edge leads to the emergence of a horseshoe vortex that collapses further downstream. These shed vortices penetrate the tip gap of the next blade under the influence of the strong tip leakage flow. In this way, they disturb the neighbouring horseshoe vortex before being transported by the main flow toward the diffuser. This local unsteady vortex shedding phenomenon is observed almost identically in every blade passage but does not significantly affect the stage performances. These disturbances can be observed on the static pressure spectrum, as illustrated in Figure 6. The plotted spectra are from a probe located close to the casing wall at $M_x = 0.42$. At OP2, the phenomenon described earlier causes an increase in pressure oscillations within the frequency range between the passing frequencies of the splitter blades and the main blades. During further throttling, the main TLV moves away from the splitter blade, driving the compressor to a stable operating point, while remaining in the negative slope section of the characteristic curve. Hence, the spectrum related to the OP3 signal reveals a stabilised flow field in which pressure fluctuations remain lower than those observed at OP2. Consequently, even if the disturbance observed near the peak efficiency seems to have rotating instability features, it must not be interpreted as a stall precursor signature.

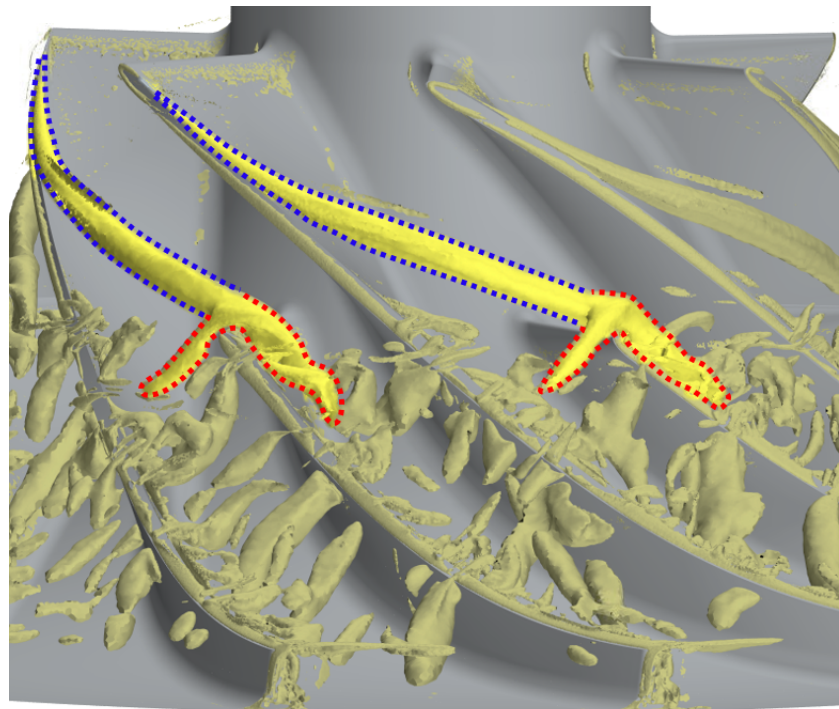


Figure 5. Iso-surfaces of λ_2 criterion at OP2.

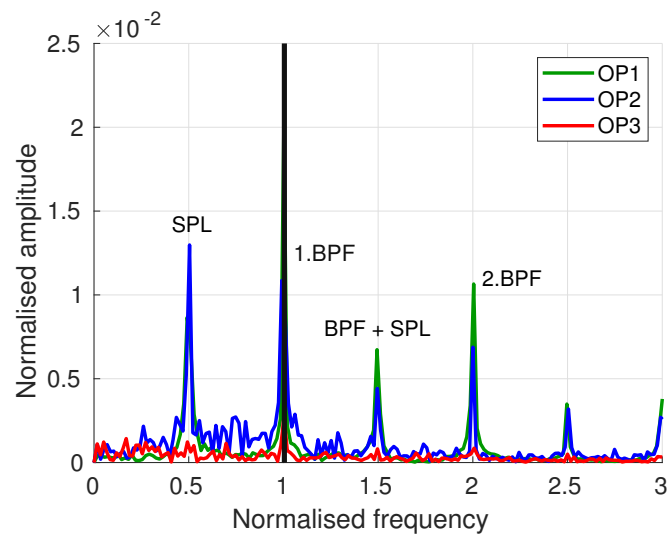


Figure 6. Static pressure spectra from the region of the splitter blade's leading edge ($M_x = 0.42$).

3.2. Flow Structures at Design Conditions

This interaction was observed in the simulations of Iwakiri et al. [11] in an impeller of a transonic compressor in near-stall conditions. Nonetheless, this previous study identified this phenomenon as one of the causes of the compressor performance reduction close to the zero slope part of the characteristic curve. In the present case, these vortical structures occurred earlier on the compressor's characteristic curve than the ones mentioned by Mitsubishi researchers. This could be explained by the geometry differences between the two configurations. Indeed, the present compressor has a wider tip gap than the impeller analysed by Iwakiri. Compared to the blade height, the present geometry has a tip clearance that is more than five times larger at the impeller inlet and around twice as large at the outlet. Through large eddy simulations, You et al. [18] demonstrated that increasing the tip gap size increases the angle between the blade and the tip leakage vortex. This could explain why the current compressor presented this unsteady interaction earlier on the

characteristic curve than the one studied by Iwakiri. Furthermore, the present splitter blades are shorter than those used in the configuration described by Iwakiri. As a result, the loss mechanisms at OP2 are confined to the region under the splitter blades' leading edges ($M_x > 0.31$), while the ones observed in Mitsubishi's compressor occurred on most of the passage's length. This also explains why the present compressor operating at OP2 provides enough work to keep the characteristic slope unchanged, whereas the one studied by Iwakiri shows performance reductions. However, considering the proximity of the best efficiency operating point, it can be assumed that OP2 would be the peak efficiency point without this phenomenon. Therefore, the angle between the tip leakage vortex and the blade's suction side must be considered when designing splitter blades, especially for impellers with wide tip clearances.

4. Backflow Vortices Emergence

4.1. Flow Structures in Near-Stall Conditions

With the decrease in the mass flow rate, the present compressor reaches the operating point, OP3, in which the TLV rolls up earlier near the main blade's leading edge and becomes shorter than those observed at OP2. According to Tan et al. [19], the angle defining the tip leakage vortex's trajectory from the main blade suction side increases with the blade loading. Furthermore, as reported by Zhang et al. [20], the reverse tip clearance flow at the impeller's outlet extends further upstream until it reaches a meridional position of $M_x = 0.1$. Figure 7 shows that at this operating point, some notable vortices emerge in front of the TLV tail before propagating in the passage. The upstream extremities of the released vortices are slightly oriented upstream, while the lower extremities remain attached to the blade's suction side. In this way, these large structures, oriented perpendicular to the streamwise direction, propagate downstream until they hit the splitter blades' leading edges. Moreover, this phenomenon proves to be periodic, and for the present mass flow rate, those vortices strike the splitter blade's leading edge approximately once per revolution. During the oncoming flow, these vortex tubes occurring at $M_x = 0.2$ occupy around the 15% of the span. Such vortices are highly similar to flow structures arising from the tip leakage flow breakdown described by Cao et al. [10]. However, the present case shows the coexistence of these wide vortices with an established tip leakage vortex.

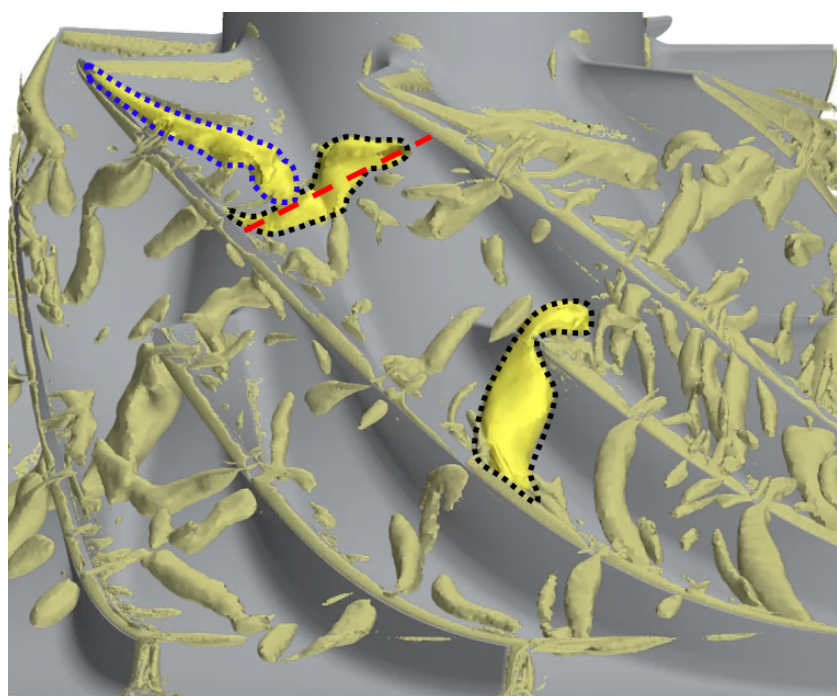


Figure 7. Iso-surfaces of λ_2 criterion at OP3.

4.2. Flow Structures in Stall Conditions

With further throttling, the compressor reaches the operating point OP4, where the interface between the tip clearance and incoming flows is parallel to the leading edges. For this mass flow, the TLV still rolls up at the main blade's leading edge, but it is shorter and tends to align with the leading edges' plane. Furthermore, the reverse tip clearance flow moves further upstream until it reaches the main blades' leading edges. In these conditions, the tip leakage vortex is sheared by the underlying axial flow and the tip gap backflow. As a result, the tip leakage vortices break down in some passages, causing the massive vortex shedding shown in Figure 8. The flow topology at this operating point closely resembles the field structures described by Cao et al. The shed vortices are similar to those observed at OP3, but they roll up nearer to the impeller inlet ($M_x = 0.08$), are oriented more diagonally upstream and are larger by around 33% span for the biggest ones. Besides, the emergence frequency of large-scale vortices has increased so that the shed vortices hit the splitter blades' leading edges between two and three times per revolution. Moreover, the upstream end is now associated with a high tangential velocity zone and propagates circumferentially. Thus, this part reaches the pressure side of the adjacent blade before passing through the tip gap and disturbing the flow structures in the next passage. This new mechanism disturbing the flow field in the neighbouring passage is illustrated in Figure 9. At (t_0) , a vortex tube (black) emerges from under the tip leakage vortex (blue). At $(t_0 + 40\Delta t)$, its upper part has moved circumferentially, while the downstream extremity is advected by the main flow. At $(t_0 + 80\Delta t)$, the upstream part passes through the next tip gap. At $(t_0 + 120\Delta t)$, the part remaining in the first passage is advected downstream toward the splitter blade's leading edge, whereas the other interacts with the neighbouring TLV. Thus, this interaction breaks the following tip leakage vortex and contributes to the creation of a new large vortex oriented perpendicular to the blade in the next passage. At the same time, the advected downstream parts of the vortices hit the splitter blades' leading edges, causing substantial pressure fluctuations.

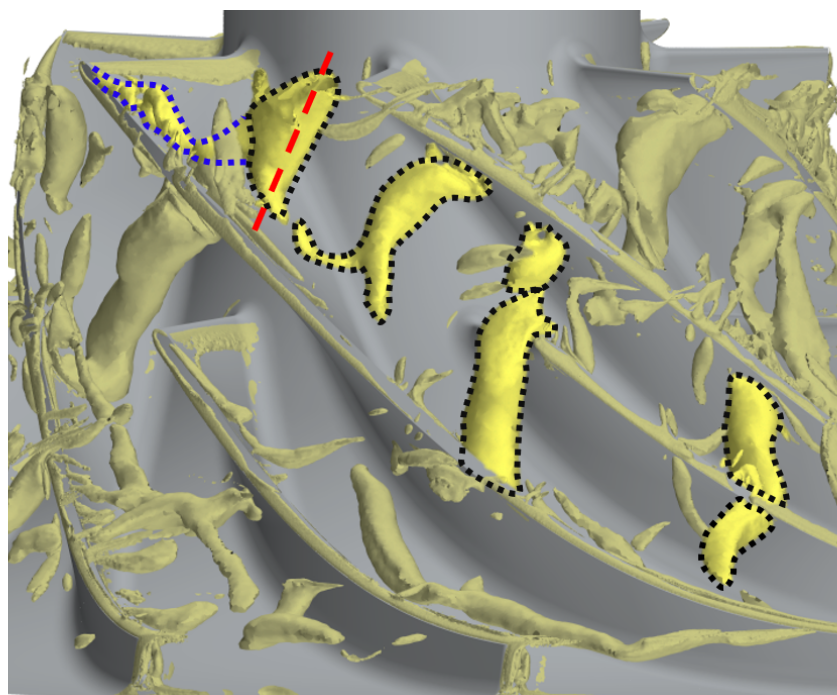


Figure 8. Iso-surfaces of λ_2 criterion at OP4.

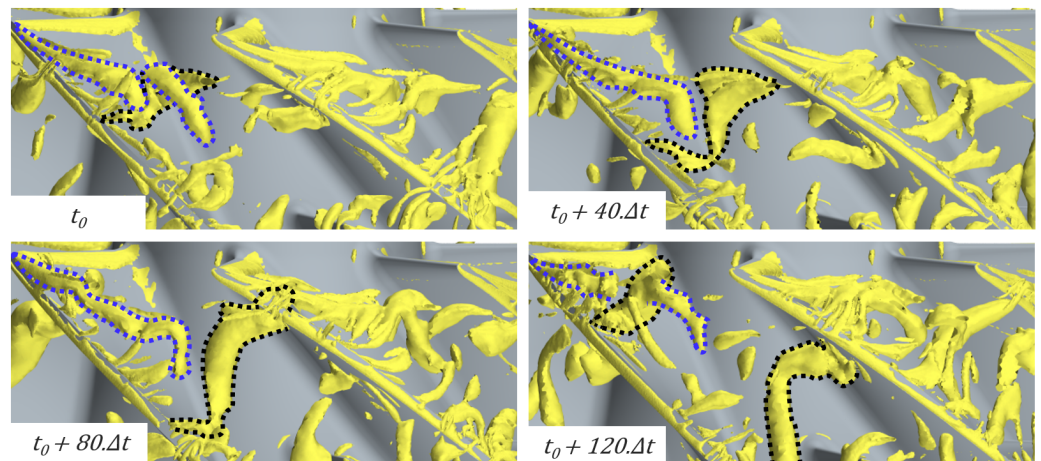


Figure 9. Large-scale vortices disturbing the neighbouring passage (OP4).

Previous works [2,4–6,21] on axial configurations have referred to these kinds of pre-stall disturbances as rotating instability. These instabilities are mainly encountered in compressors with wide tip clearances operating in near-stall conditions. As reported by Day [22], they are defined by their small size (about one pitch), low-pressure spots moving from the suction of a blade to the pressure side of the next one, and by a characteristic hump (about one-third of the blade’s passing frequency) on frequency spectra. A Fourier transform has been performed on the pressure signal recorded by a fixed probe located at $M_x = 0.09$ to identify the present instabilities. Figure 10 shows the related frequency spectrum in which abscissa has been normalised by the main blade’s passing frequency (BPF). A distinctive hump is observed around one-third of the BPF, strengthening the rotating instability assumption. The discrete peak located just under one-third of the BPF is related to the passage of the vortex tubes that propagate circumferentially close to the leading edges.

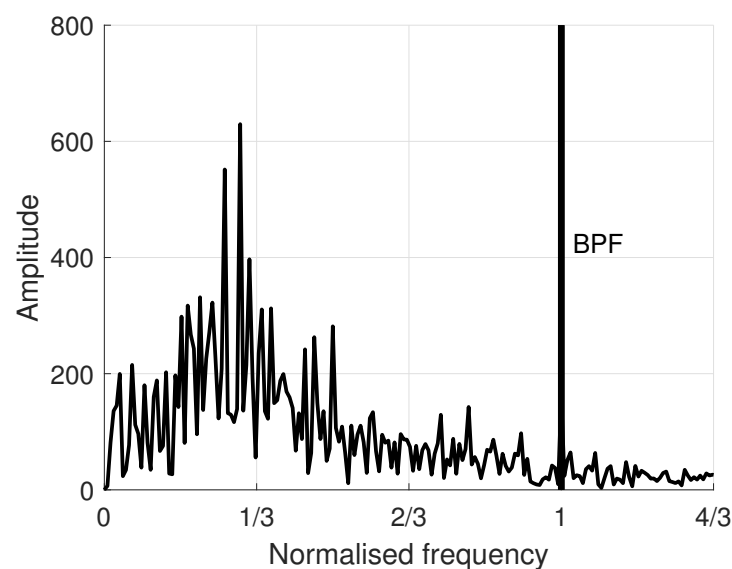


Figure 10. Static pressure spectrum from the tip region of the main blade’s passage at OP4 ($M_x = 0.09$).

Some passages are ahead of the instabilities development. Indeed, passages coexist simultaneously with collapsed tip leakage vortices and ones with stable TLV in the impeller. The passages with broken TLV were noted to be associated with large vortical structures aligned with the leading edges’ plane. In contrast, the passages linked to unbroken TLV

contain thin structures that roll up further downstream. This last flow topology is similar to the flow field observed at a higher mass flow rate when the compressor operates at OP3. This phenomenon is due to the non-uniformity of the pressure distribution induced by the volute in the vaneless diffuser. The asymmetry of the volute leads to a high-pressure region in front of the volute’s tongue, followed by a low-pressure zone. Figure 11 outlines the non-uniformity of the flow field in the vaneless diffuser by plotting the time-averaged static pressure variations, \tilde{P}_S , around the impeller, where $P_S(\theta, t_k)$ is the static pressure in the vaneless diffuser at t_k and $\overline{P}_S(t_k)$ is the circumferential average of $P_S(\theta, t_k)$.

This downstream distortion that ramps up with the mass flow reduction causes a periodic disturbance that drives the development of the instabilities in the impeller passages. In agreement with Zhang et al. [20], the potential effect propagates upstream through the subsonic flow until it reaches the plane of the main blades’ leading edges. This mechanism explains the instant disparity of tip leakage vortices’ behaviours in the different rotor passages.

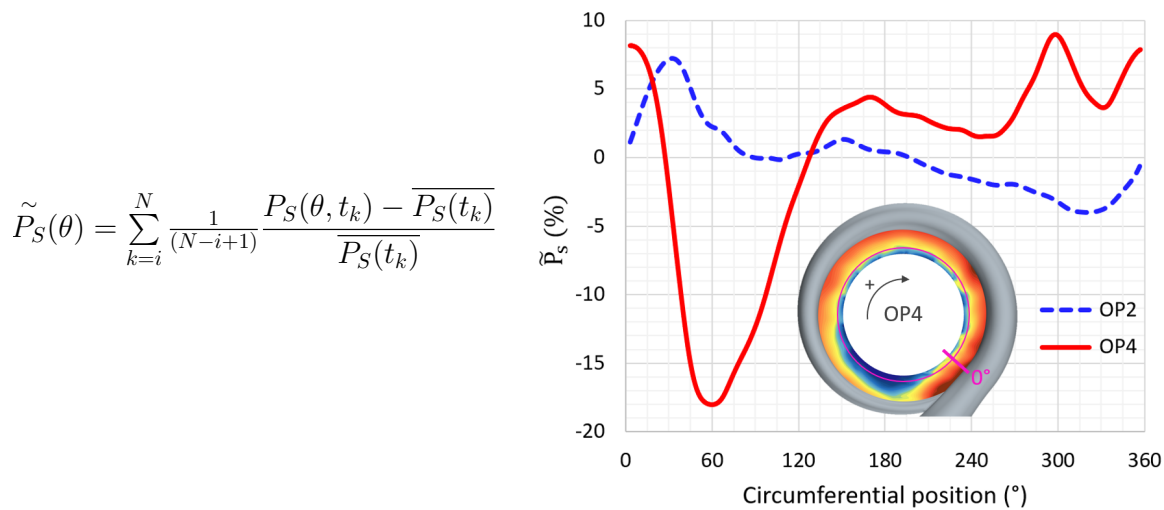


Figure 11. Volute influence on pressure distribution in the diffuser near impeller trailing edges.

4.3. Backflow Vortices Inception Mechanisms

Cao et al. [10] assumed that these large vortices are induced by a Kelvin–Helmholtz instability of the shear layer formed between the main-stream flow and the tip leakage flow. However, this theory does not explain the vortex tube orientation. The first vortex rolling up caused by a Kelvin–Helmholtz instability of a shear layer in a centrifugal compressor was described by Bousquet et al. [9]. In this work, the shed vortices extended radially from the blade’s suction side to the casing wall without growing diagonally upstream or being aligned perpendicular to the blade. Furthermore, the tip leakage flow breakdown process described by Cao is incompatible with the coexistence of a stable TLV and a vortex tube shedding, as observed at OP3. This fact encouraged further study of the mechanisms behind the present flow structures. A similar flow pattern was experimentally observed within an axial compressor by Chen et al. [14]. They refer to this vortical structure as the backflow vortex (BFV) and describe it as a filament that emerges from the bottom of the TLV near the blade’s leading edge. The explanation set out in this study is that a shear layer exists under the tip leakage vortex whose primary vorticity direction is such as if this layer has to roll up, then it will roll up perpendicularly to the blade. They also suggest that the shear layer rolling up is triggered by the interaction between the main incoming flow under it and the reverse flow close to the shroud, hence the name, backflow vortex.

To compare the present flow field (at OP3) with the one analysed by the Baltimore research team, the relative velocity components around the tip leakage vortex are shown in Figure 12. The displayed components are expressed in the rotating frame (e_r, e_θ, e_x) and are normalised by a reference blade speed defined as $U_{ref} = \omega \cdot r_{tip}$. In accordance with

the analysis conducted by Chen et al. [14] on the axial configuration, Figure 12 reveals the coexistence of two distinct regions *A* and *B* around the tip leakage vortex. The first one, located near the TLV centre, is characterised by a high relative tangential velocity W_θ and a negative axial velocity W_x . The second one is observed under the TLV and, contrary to the region *A*, has a low tangential component associated with a high axial component related to the blockage effect induced by the tip leakage vortex. Both have similar radial velocities, but there are significant radial gradients in W_θ and W_x between the two zones. Figure 12 also outlines that the resulting relative velocity (between *B* and *A*) W_{B-A} is parallel to the blade's suction side. As the vorticity is defined by the curl of the velocity field, the resultant of the vorticity components around the shear layer is aligned perpendicular to the blade. Furthermore, W_x distribution demonstrates that, in our case, the shear layer rolling up is probably caused by the influence of the upper reverse flow from the tip clearance and the forward main flow under it. This flow pattern, which is highly similar to the one highlighted by Chen, agrees with the vortical structures observed in the present centrifugal compressor. Therefore, from now on, the massive vortex tubes observed at OP3 and OP4 aligned perpendicular to the blade will be named “backflow vortices”.

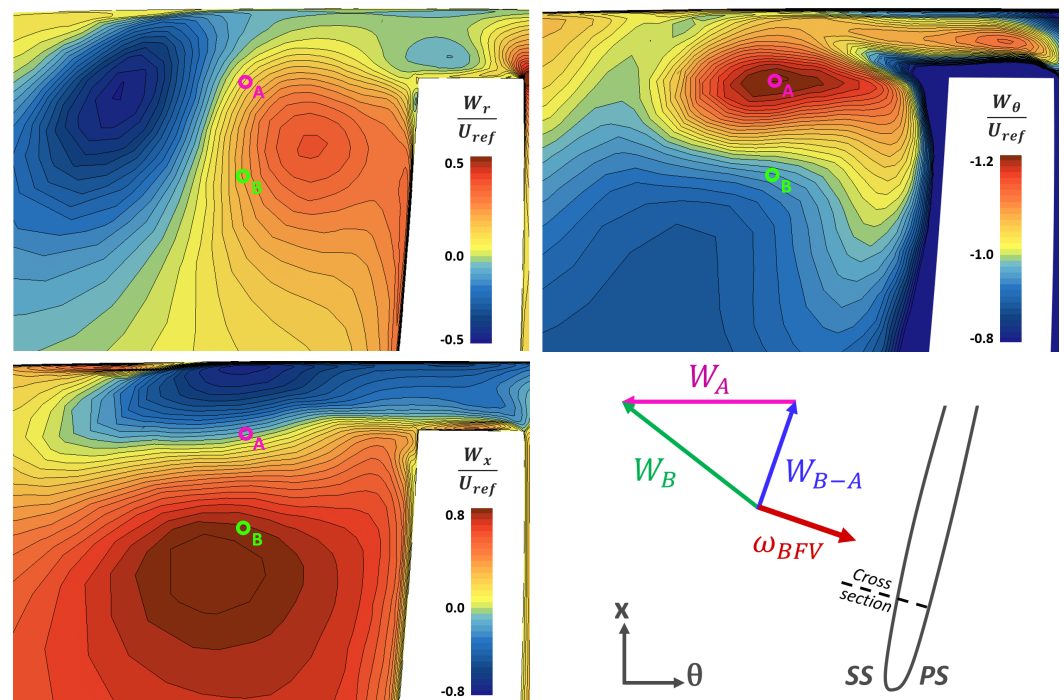


Figure 12. Relative velocity components plotted on a cross-section in the tip region (OP3 – $M_x = 0.08$).

5. Conclusions

Based on the flow mechanisms reported here, unsteady three-dimensional calculations of the full compressor stage are required to simulate the rotating instability onset. The first operating points analysis has shown that even during design conditions, this kind of geometry with wide tip clearances leads to unsteady loss mechanisms due to the interaction between the main blade's tip vortex and the splitter blade. Hence, this phenomenon must be considered during the design of the splitter blades. Then, at lower mass flow rates, the highlight of the relative tangential velocity radial gradient under the TLV complements the previous study of the large-scale vortex shedding carried out at the Whittle Laboratory. Furthermore, it has been brought to light that the volute's shape significantly impacts the axisymmetric balance that drives the development of instabilities in the impeller passages. The vortices reported here lead to a significant increase in the incidence angle in the tip region. It is thus interesting to study the role of these structures in the stall inception.

Author Contributions: Conceptualization, X.F., N.B., Y.B. and S.C.; methodology, X.F., N.B., Y.B. and S.C.; validation, X.F., N.B., Y.B. and S.C.; formal analysis, X.F.; investigation, X.F.; data curation, X.F.; writing—original draft preparation, X.F.; writing—review and editing, X.F., N.B., Y.B. and S.C.; visualization, X.F.; supervision, N.B., Y.B. and S.C.; project administration, N.B., Y.B. and S.C.; funding acquisition, N.B., Y.B. and S.C. All authors have read and agreed to the published version of the manuscript.

Funding: This work was funded by Liebherr-Aerospace Toulouse S.A.S.

Data Availability Statement: The data presented in this study are available upon request from the corresponding author.

Acknowledgments: The authors would like to thank Liebherr Aerospace Toulouse S.A.S for supporting the present research program. The researchers was granted access to the HPC resources of CINES under the allocation 2023-A0132A06879 made by GENCI and to the HPC resources of CALMIP supercomputing centre under the allocation 2023-P18021.

Conflicts of Interest: The authors declare no conflict of interest.

Abbreviations

The following abbreviations are used in this manuscript:

BFV	Backflow Vortex.
BPF	Blade Passing Frequency.
SPL	Splitter blade.
TLV	Tip Leakage Vortex.
V_i	Absolute velocity component on direction 'i'.
W_i	Relative velocity component on direction 'i'.
M_x	Relative meridional position.
ω_{BFV}	Backflow vortex primary vorticity.

References

- Inoue, M.; Kuroumaru, M. Structure of Tip Clearance Flow in an Isolated Axial Compressor Rotor. *J. Turbomach.* **1989**, *111*, 250–256. [[CrossRef](#)]
- Inoue, M.; Kuroumaru, M.; Iwamoto, T.; Ando, Y. Detection of a Rotating Stall Precursor in Isolated Axial Flow Compressor Rotors. *J. Turbomach.* **1991**, *113*, 281–287. [[CrossRef](#)]
- Inoue, M.; Kuroumaru, M.; Tanino, T.; Furukawa, M. Propagation of Multiple Short-Length-Scale Stall Cells in an Axial Compressor Rotor. *J. Turbomach.* **1999**, *122*, 45–54. [[CrossRef](#)]
- Inoue, M.; Kuroumaru, M.; Tanino, T.; Yoshida, S.; Furukawa, M. Comparative Studies on Short and Long Length-Scale Stall Cell Propagating in an Axial Compressor Rotor. *J. Turbomach.* **2000**, *123*, 24–30. [[CrossRef](#)]
- März, J.; Hah, C.; Neise, W. An Experimental and Numerical Investigation into the Mechanisms of Rotating Instability. *J. Turbomach.* **2002**, *124*, 367–374. [[CrossRef](#)]
- Mailach, R.; Lehmann, I.; Vogeler, K. Rotating Instabilities in an Axial Compressor Originating From the Fluctuating Blade Tip Vortex. *J. Turbomach.* **2000**, *123*, 453–460. [[CrossRef](#)]
- Vo, H.D.; Tan, C.S.; Greitzer, E.M. Criteria for spike initiated rotating stall. *J. Turbomach.* **2008**, *130*, 011023. [[CrossRef](#)]
- Pullan, G.; Young, A.M.; Day, I.J.; Greitzer, E.M.; Spakovszky, Z.S. Origins and Structure of Spike-Type Rotating Stall. *J. Turbomach.* **2015**, *137*, 051007. [[CrossRef](#)]
- Bousquet, Y.; Binder, N.; Dufour, G.; Carbonneau, X.; Roumeas, M.; Trébinjac, I. Numerical simulation of stall inception mechanisms in a centrifugal compressor with vaned diffuser. *J. Turbomach.* **2016**, *138*, 121005. [[CrossRef](#)]
- Cao, T.; Kanzaka, T.; Xu, L.; Brandvik, T. Tip Leakage Flow Instability in a Centrifugal Compressor. *J. Eng. Gas Turbines Power* **2021**, *143*, 041012. [[CrossRef](#)]
- Iwakiri, K.; Furukawa, M.; Ibaraki, S.; Tomita, I. Unsteady and three-dimensional flow phenomena in a transonic centrifugal compressor impeller at rotating stall. In Proceedings of the ASME Turbo Expo 2009: Power for Land, Sea, and Air, Orlando, FL, USA, 8–12 June 2009; Volume 48883, pp. 1611–1622. [[CrossRef](#)]
- Tomita, I.; Ibaraki, S.; Furukawa, M.; Yamada, K. The Effect of Tip Leakage Vortex for Operating Range Enhancement of Centrifugal Compressor. *J. Turbomach.* **2013**, *135*, 051020. [[CrossRef](#)]
- Flete, X.; Binder, N.; Bousquet, Y.; Cros, S. Numerical investigation of rotating instabilities development in a wide tip gap centrifugal compressor. In Proceedings of the 15th European Turbomachinery Conference, Budapest, Hungary, 24–28 April 2023; Paper n. ETC2023-119. Available online: <https://www.euroturbo.eu/publications/conference-proceedings-repository/> (accessed on 7 June 2023)

14. Chen, H.; Li, Y.; Tan, D.; Katz, J. Visualizations of Flow Structures in the Rotor Passage of an Axial Compressor at the Onset of Stall. In Proceedings of the ASME Turbo Expo 2016: Turbomachinery Technical Conference and Exposition, Seoul, Republic of Korea, 13–17 June 2016. [[CrossRef](#)]
15. Menter, F.R. Two-equation eddy-viscosity turbulence models for engineering applications. *AIAA J.* **1994**, *32*, 1598–1605.
16. Kulak, M.; Grapow, F.; Liśkiewicz, G. Numerical analysis of centrifugal compressor operating in near-surge conditions. *J. Phys. Conf. Ser.* **2018**, *1101*, 012017. [[CrossRef](#)]
17. Jeong, J.; Hussain, F. On the identification of a vortex. *J. Fluid Mech.* **1995**, *285*, 69–94. [[CrossRef](#)]
18. You, D.; Wang, M.; Moin, P.; Mittal, R. Effects of tip-gap size on the tip-leakage flow in a turbomachinery cascade. *Phys. Fluids* **2006**, *18*, 105102. [[CrossRef](#)]
19. Tan, D.; Li, Y.; Chen, H.; Wilkes, I.; Katz, J. The Three Dimensional Flow Structure and Turbulence in the Tip Region of an Axial Flow Compressor. In Proceedings of the ASME Turbo Expo 2015: Turbine Technical Conference and Exposition, Montreal, QC, Canada, 15–19 June 2015. [[CrossRef](#)]
20. Zhang, H.; Yang, C.; Shi, X.; Yang, C.; Chen, J. Two stall stages in a centrifugal compressor with a vaneless diffuser. *Aerosp. Sci. Technol.* **2021**, *110*, 106496. [[CrossRef](#)]
21. Young, A.; Day, I.; Pullan, G. Stall Warning by Blade Pressure Signature Analysis. *J. Turbomach.* **2012**, *135*, 011033. [[CrossRef](#)]
22. Day, I. Stall, surge, and 75 years of research. *J. Turbomach.* **2016**, *138*, 011001. [[CrossRef](#)]

Disclaimer/Publisher’s Note: The statements, opinions and data contained in all publications are solely those of the individual author(s) and contributor(s) and not of MDPI and/or the editor(s). MDPI and/or the editor(s) disclaim responsibility for any injury to people or property resulting from any ideas, methods, instructions or products referred to in the content.